Electronic Supporting Information

Composition regulation of ternary rare earth halide solid-state electrolytes and its influence on ionic conducting and electrochemical properties

Anyi Zheng[a,b], Liang Luo[a,b], Linwei Li[a,b], Zhouqing Jiang[a,b], Shengming Ma[a,b], Jinqiu Yu[a,b,*]

a. Rare Earth Functional Materials (Xiong'an) Innovation Center Co., Ltd., Xiong'an 071700, China
b. National Engineering Research Center for Rare Earth, Grirem Advanced Materials Co., Ltd., Beijing 100088, China

*Corresponding Authors: yujinqiu@mail.ipc.ac.cn (Jinqiu Yu)

1. Materials and experiments

1.1 Preparation of the ternary rare earth halide SSEs

$Li_3YCl_{6-x}Br_x$ (x=0, 1.2, 2.4, 3.6, 4.8, 6) were synthesized according to reactions (1) and (2). $Li_3YBr_{6-x}I_x$ (x=1.2, 2.4, 3.6, 4.8, 6) were synthesized according to reactions (3) and (4). Raw mateirals of LiX (LiCl, LiBr, LiI, Grirem Advanced Materials Co., Ltd., 99.99%) and YX_3 (YCl_3, YBr_3, YI_3, Grirem Advanced Materials Co., Ltd., 99.99%) were weighted and ground in agate mortars in an Ar-filled glove box with O_2 and H_2O contents less than 1 ppm. Stoichiometric mixtures of precursors were sealed in a quartz ampoule under vacuum and then heated in a furnace at 600℃ for 10h. Then the ampoule was cooled to room temperature at a cooling rate of about 4℃/min and taken into the glovebox. $Li_3YCl_{6-x}Br_x$ (x=0, 1.2, 2.4, 3.6, 4.8, 6) and $Li_3YBr_{6-x}I_x$ (x=1.2, 2.4, 3.6, 4.8, 6) products were harvested from the ampoule and ground into powders for characterization.

Li_xMCl_{3+x} (M=Y, Dy, Ho, Er, Tm, Yb, Lu; x=2.8, 3) were prepared according to the reaction (5) using LiCl and MCl_3 (YCl_3, $DyCl_3$, $HoCl_3$, $ErCl_3$, $TmCl_3$, $YbCl_3$, $LuCl_3$, Grirem Advanced Materials Co., Ltd., 99.99%) as raw materials by the same method.

(1) $(3-x)LiCl + xLiBr + YCl_3 \rightarrow Li_3YCl_{6-x}Br_x$ (x=0, 1.2, 2.4)

(2) $(6-x)LiCl + (x-3)LiBr + YBr_3 \rightarrow Li_3YCl_{6-x}Br_x$ (x=3.6, 4.8, 6)

(3) $(3-x)LiBr + xLiI + YBr_3 \rightarrow Li_3YBr_{6-x}I_x$ (x=1.2, 2.4)

(4) $(6-x)LiBr + (x-3)LiI + YI_3 \rightarrow Li_3YBr_{6-x}I_x$ (x=3.6, 4.8, 6)

(5) $xLiCl + MCl_3 \rightarrow Li_xMCl_{3+x}$ (x=2.8, 3)

1.2 Powder X-ray Diffraction

The patterns of powder X-ray diffraction (XRD) were collected on a Regaku Smartlab diffractometer using Co-Kα1 X-ray source. The powder samples were prepared in an Ar-filled glove box and sealed into a special designed hermetical sample holder with polyimide tapes, which can avoid moisture contamination during the transportation and measurement. Diffraction patterns were collected with a scanning speed of 2°/min with the range of 15°-80° at room temperature.

1.3 Measurements of electrochemical properties

The ionic conductivities were measured by electrochemical impedance spectroscopy

(EIS) using an INTELLO (VIONIC) electrochemical workstation. The EIS patterns were collected in a frequency range from 1 Hz to10 MHz. 150-200 mg of ground samples were pressed into pellets with 10mm diameter at 400 MPa and blocked with stainless steel rod electrodes for measurement. The external pressure keeps 400 MPa during the EIS tests. The tests were all conducted at room temperature of 25℃. The activation energies were determined according to the Arrhenius equation of $\sigma=A\cdot\exp(-E_a/RT)$, where σ, E_a, R, T, A is the ionic conductivity (obtained at 278.15, 288.15, 298.15, 308.15, 318.15, 328.15, 338.15 K), activation energy, ideal gas constant (8.314J/(K·mol)), kelvin temperature, pre-exponential factor, respectively.

The electronic conductivities of the samples were measured by chrono amperometry (constant potential) with voltage of 1V and duration time of 3600s. The values are calculated by $\sigma_e=I_e\cdot L/(V\cdot A)$, where I_e, L, V, A is the equilibrium current, the thickness of the sample, the applied voltage, and the area of the sample pellet, respectively.

The electrochemical stability window was measured by linear sweep voltammetry (LSV) in a range of 0~6 V Li^+/Li at 1 mV/s using a Bio-Logic SAS electrochemical workstation with a BE/L-M-X+C/L-M-X/$Li_{5.5}PS_{4.5}Cl_{1.5}$/Li cell, where BE represents a stainless-steel blocking electrode, L-M-X represents a rare earth halide SSE, C represents the conductive carbon additive. The cell was fabricated as follows: First, 60 mg of $Li_{5.5}PS_{4.5}Cl_{1.5}$ powders were placed into a polytetrafluoroethylene (PTFE) die with diameter of 10 mm and then compressed into a pellet at 130 MPa. Second, 60 mg of as-synthesized rare earth halide SSE powders were added evenly on one side of the $Li_{5.5}PS_{4.5}Cl_{1.5}$ pellet and then they were pressed together at 260 MPa. Third, 10 mg of composites of the rare earth halide SSE and conductive carbon with a mass ratio of 70:30 were added evenly on the halide SSE side of the pellet and further pressed at 400 MPa. Finally, a Li metal rod with diameter of 10 mm was added to the $Li_{5.5}PS_{4.5}Cl_{1.5}$ side while a stainless steel blocking rod was added to the rare earth halide SSE side, and they were compressed at 50 MPa to form the cell.

The ASSB cells were assembled in the configuration of In-Li/$Li_{5.5}PS_{4.5}Cl_{1.5}$/halide-SSE/SSE-NCM88. The assembling process is as follows: (1) 60 mg of $Li_{5.5}PS_{4.5}Cl_{1.5}$ was placed into a polytetrafluoroethylene (PTFE) die with diameter of 10 mm, and then

was compressed at 200 MPa to form a pellet. (2) 60 mg of the as-synthesized halide SSE was added on one side of the $Li_{5.5}PS_{4.5}Cl_{1.5}$ pellet and then compressed at 400 MPa. (3) 10 mg of cathode mixture of single-crystalline $LiNi_{0.88}Co_{0.09}Mn_{0.03}O_2$ powders, as-prepared halide electrolyte and Super P carbon with a mass ratio of 70:30:1 was spread on the halide SSE side and further pressed at 600 MPa. (4) A slice of In metal with a diameter of 10 mm was added to the $Li_{5.5}PS_{4.5}Cl_{1.5}$ side, and a small piece of Li metal with a weight less than 3mg was added to the In side and then compressed at 100 MPa. (5) The cell was locked in a stainless-steel frame and further tightened at 400MPa. The whole assembling process was carried out in an Ar-filled glove box with the H_2O content less than 1 ppm. Capacity and cycling performance of the cells were carried out in a potential range of 2.5-4.3 V (vs. Li/Li^+)under an continuously external pressure of 400 MPa at 25 ℃. The cells were cycled at 0.1C at the first three cycles, and cycled at 0.3C after the third cycle.

2. Results and Discussions (Table S1-S5, Fig.S1-S11)

Table S1. The calculated $r_{M/X}$ values of $Li_3YCl_{6-x}Br_x$ (x=0, 1.2, 2.4, 3.6, 4.8, 6) and $Li_3YBr_{6-x}I_x$ (x=1.2, 2.4, 3.6, 4.8, 6).

Material	Radius of M^{3+} (Å)	Radius of X^- (Å)	$r_{M/X}$
Li_3YCl_6	1.04	1.67	0.623
$Li_3YCl_{4.8}Br_{1.2}$	1.04	1.70	0.612
$Li_3YCl_{3.6}Br_{2.4}$	1.04	1.73	0.601
$Li_3YCl_{2.4}Br_{3.6}$	1.04	1.76	0.591
$Li_3YCl_{1.2}Br_{4.8}$	1.04	1.79	0.581
Li_3YBr_6	1.04	1.82	0.571
$Li_3YBr_{4.8}I_{1.2}$	1.04	1.87	0.556
$Li_3YBr_{3.6}I_{2.4}$	1.04	1.92	0.542
$Li_3YBr_{2.4}I_{3.6}$	1.04	1.96	0.531
$Li_3YBr_{1.2}I_{4.8}$	1.04	2.01	0.517
Li_3YI_6	1.04	2.06	0.505

Note 1: The radii of Y^{3+}, Cl^-, Br^- and I^- are 1.04Å, 1.67Å, 1.82Å and 2.06Å, respectively [Ref. 1, Supplementary Table 3]

Note 2: The X^- radii of mixed halides are calculated by their weighted average.

Table S2. The calculated $r_{M/X}$ values of Li_3MCl_6 (M=Y, Dy, Ho, Er, Tm, Yb, Lu).

Material	Radius of M^{3+} (Å)	Radius of X^- (Å)	$r_{M/X}$
Li_3YCl_6	1.04	1.67	0.623
Li_3DyCl_6	1.052	1.67	0.630
Li_3HoCl_6	1.041	1.67	0.623
Li_3ErCl_6	1.03	1.67	0.617
Li_3TmCl_6	1.02	1.67	0.611
Li_3YbCl_6	1.008	1.67	0.603
Li_3LuCl_6	1.001	1.67	0.599

Note 1: The radii of Y^{3+}, Dy^{3+}, Ho^{3+}, Er^{3+}, Tm^{3+}, Yb^{3+}, Lu^{3+} and Cl^- are 1.04Å, 1.052Å, 1.041Å, 1.03Å, 1.02Å, 1.008Å, 1.001Å, and 1.67Å, respectively [Ref. 1, Supplementary Table 3]

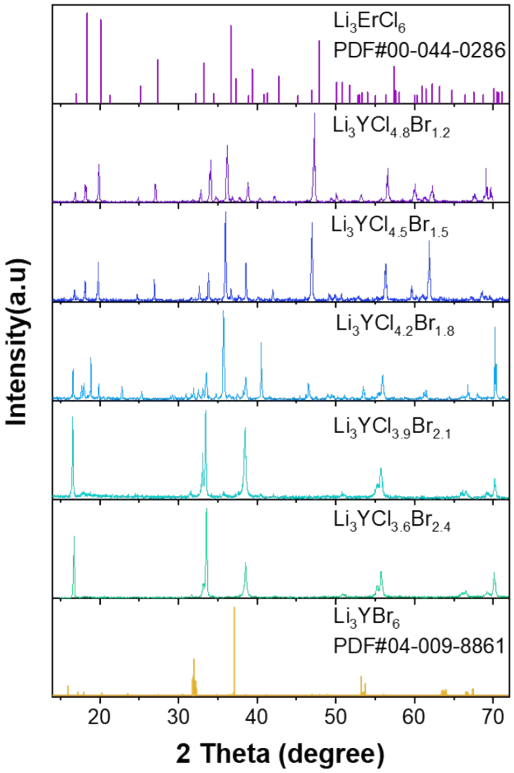

Figure S1. Powder X-ray diffraction patterns of $Li_3YCl_{6-x}Br_x$ (x=1.2, 1.5, 1.8, 2.1, 2.4).

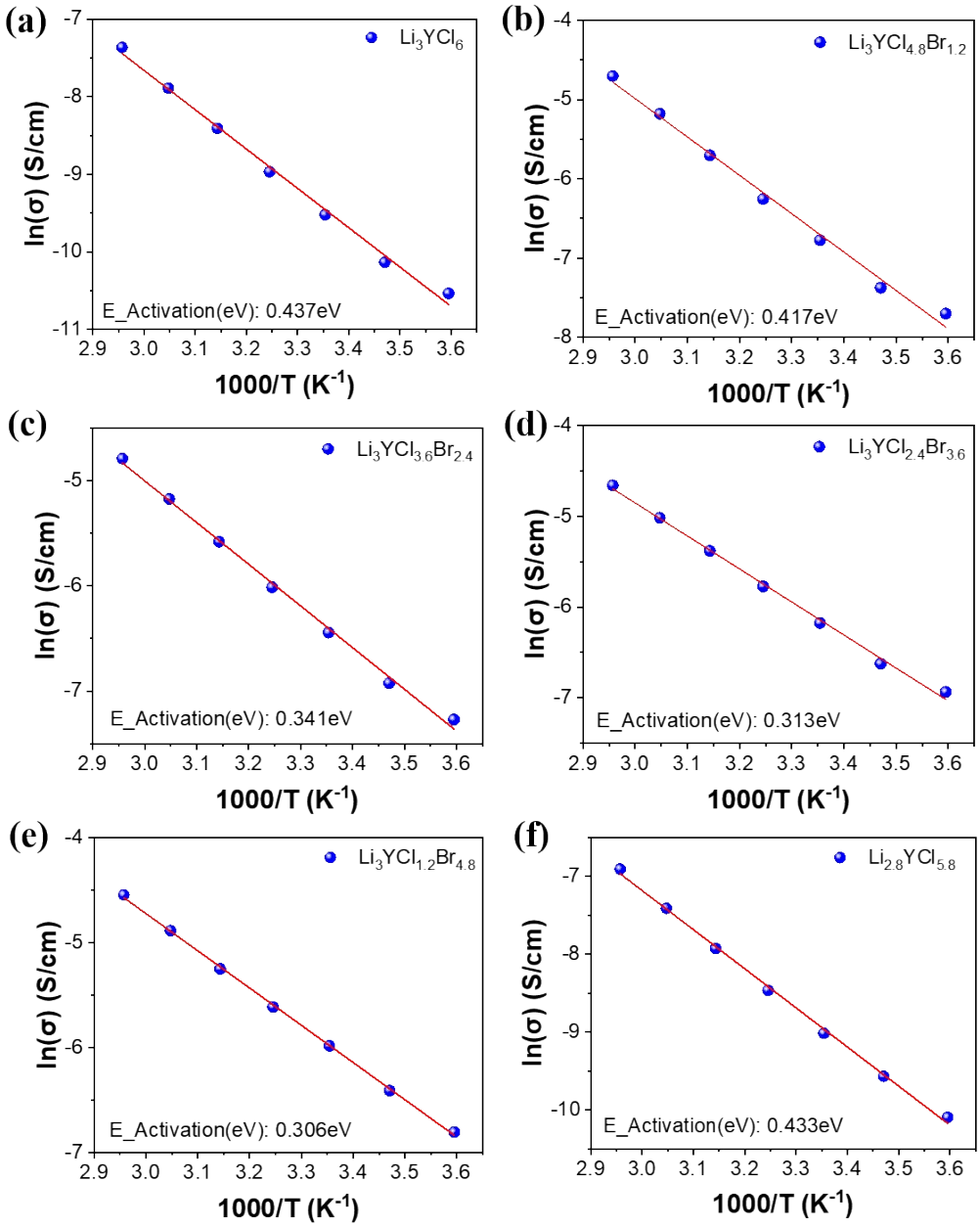

Figure S2. Arrhenius plots of (a) Li_3YCl_6, (b) $Li_3YCl_{4.8}Br_{1.2}$, (c) $Li_3YCl_{3.6}Br_{2.4}$, (d) $Li_3YCl_{2.4}Br_{3.6}$, (e) $Li_3YCl_{1.2}Br_{4.8}$, (f) $Li_{2.8}YCl_{5.8}$ as measured by EIS at different temperatures.

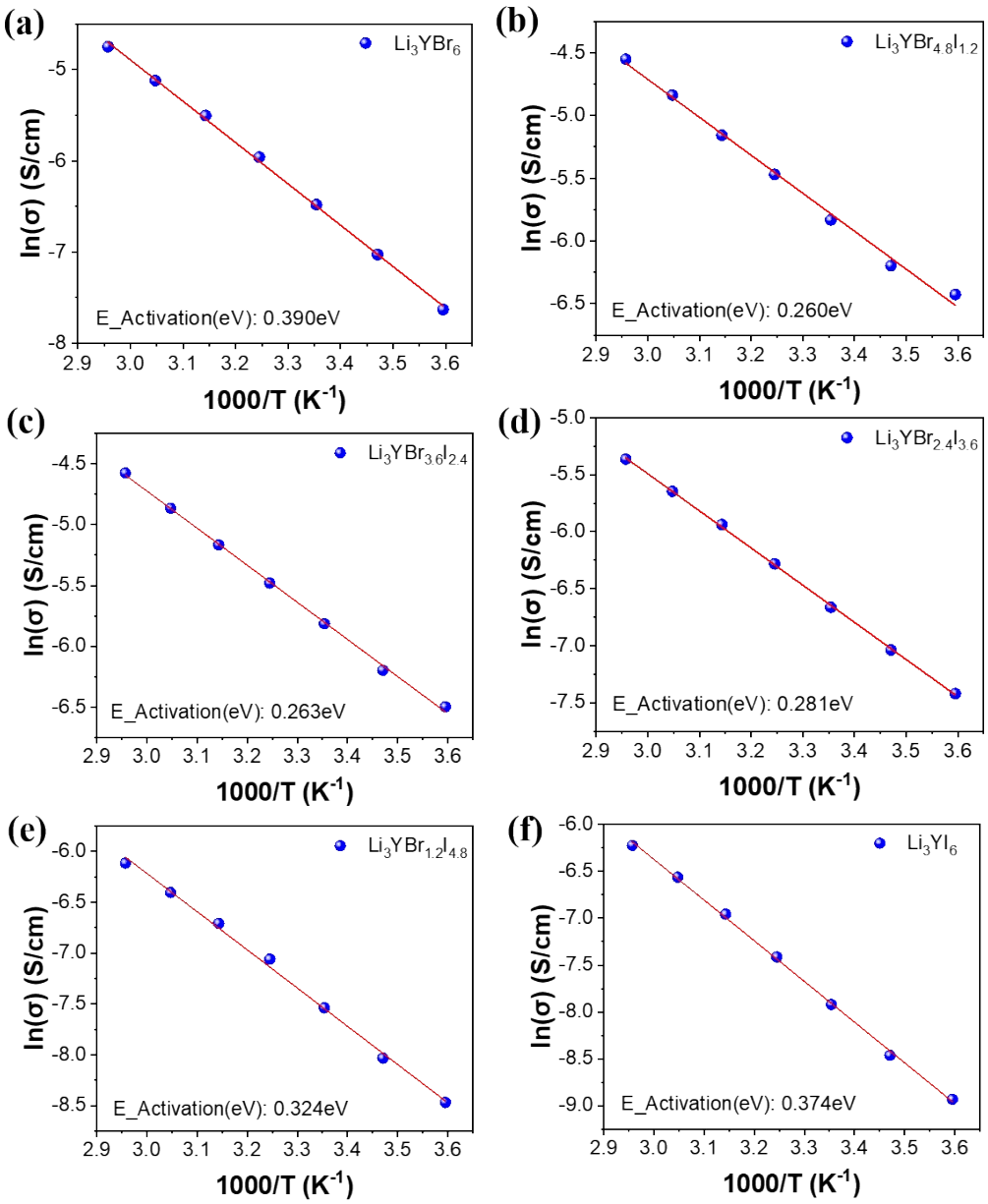

Figure S3. Arrhenius plots of (a) Li_3YBr_6, (b) $Li_3YBr_{4.8}I_{1.2}$, (c) $Li_3YBr_{3.6}I_{2.4}$, (d) $Li_3YBr_{2.4}I_{3.6}$, (e) $Li_3YBr_{1.2}I_{4.8}$, (f) Li_3YI_6 as measured by EIS at different temperatures.

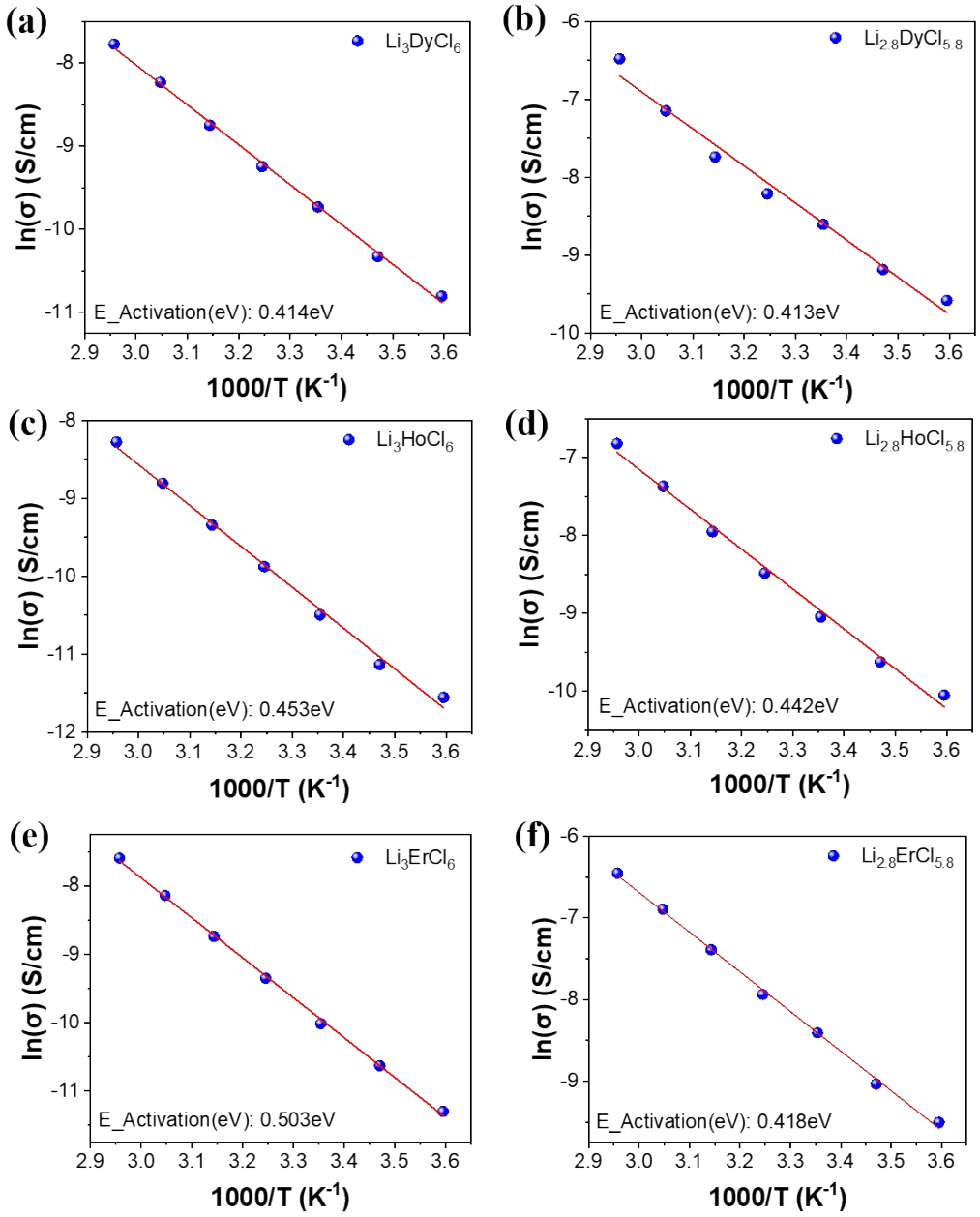

Figure S4. Arrhenius plots of (a) Li_3DyCl_6, (b) $Li_{2.8}DyCl_{5.8}$, (c) Li_3HoCl_6, (d) $Li_{2.8}HoCl_{5.8}$, (e) Li_3ErCl_6, (f) $Li_{2.8}ErCl_{5.8}$ as measured by EIS at different temperatures.

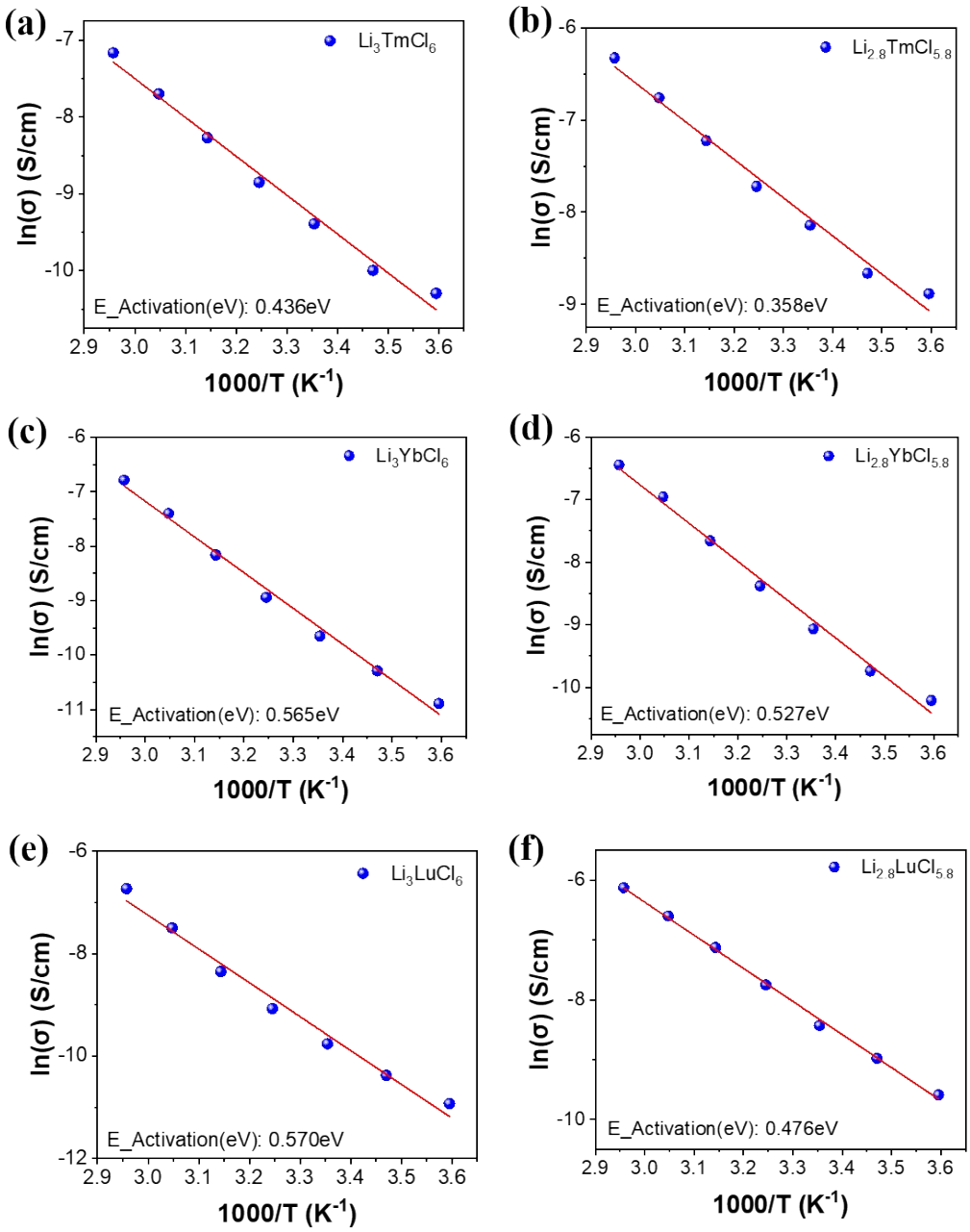

Figure S5. Arrhenius plots of (a) Li_3TmCl_6, (b) $Li_{2.8}TmCl_{5.8}$, (c) Li_3YbCl_6, (d) $Li_{2.8}YbCl_{5.8}$, (e) Li_3LuCl_6, (f) $Li_{2.8}LuCl_{5.8}$ as measured by EIS at different temperatures.

Table S3. Activation energy (E_a) of Li-M-X.

Sample	Activation energy (E_a)/eV
Li_3YCl_6	0.437
$Li_3YCl_{4.8}Br_{1.2}$	0.417
$Li_3YCl_{3.6}Br_{2.4}$	0.341
$Li_3YCl_{2.4}Br_{3.6}$	0.313
$Li_3YCl_{1.2}Br_{4.8}$	0.306
Li_3YBr_6	0.390
$Li_3YBr_{4.8}I_{1.2}$	0.260
$Li_3YBr_{3.6}I_{2.4}$	0.263
$Li_3YBr_{2.4}I_{3.6}$	0.281
$Li_3YBr_{1.2}I_{4.8}$	0.324
Li_3YI_6	0.374
$Li_{2.8}YCl_{5.8}$	0.433
Li_3DyCl_6	0.414
$Li_{2.8}DyCl_{5.8}$	0.413
Li_3HoCl_6	0.453
$Li_{2.8}HoCl_{5.8}$	0.442
Li_3ErCl_6	0.503
$Li_{2.8}ErCl_{5.8}$	0.418
Li_3TmCl_6	0.436
$Li_{2.8}TmCl_{5.8}$	0.358
Li_3YbCl_6	0.565
$Li_{2.8}YbCl_{5.8}$	0.527
Li_3LuCl_6	0.570
$Li_{2.8}LuCl_{5.8}$	0.476

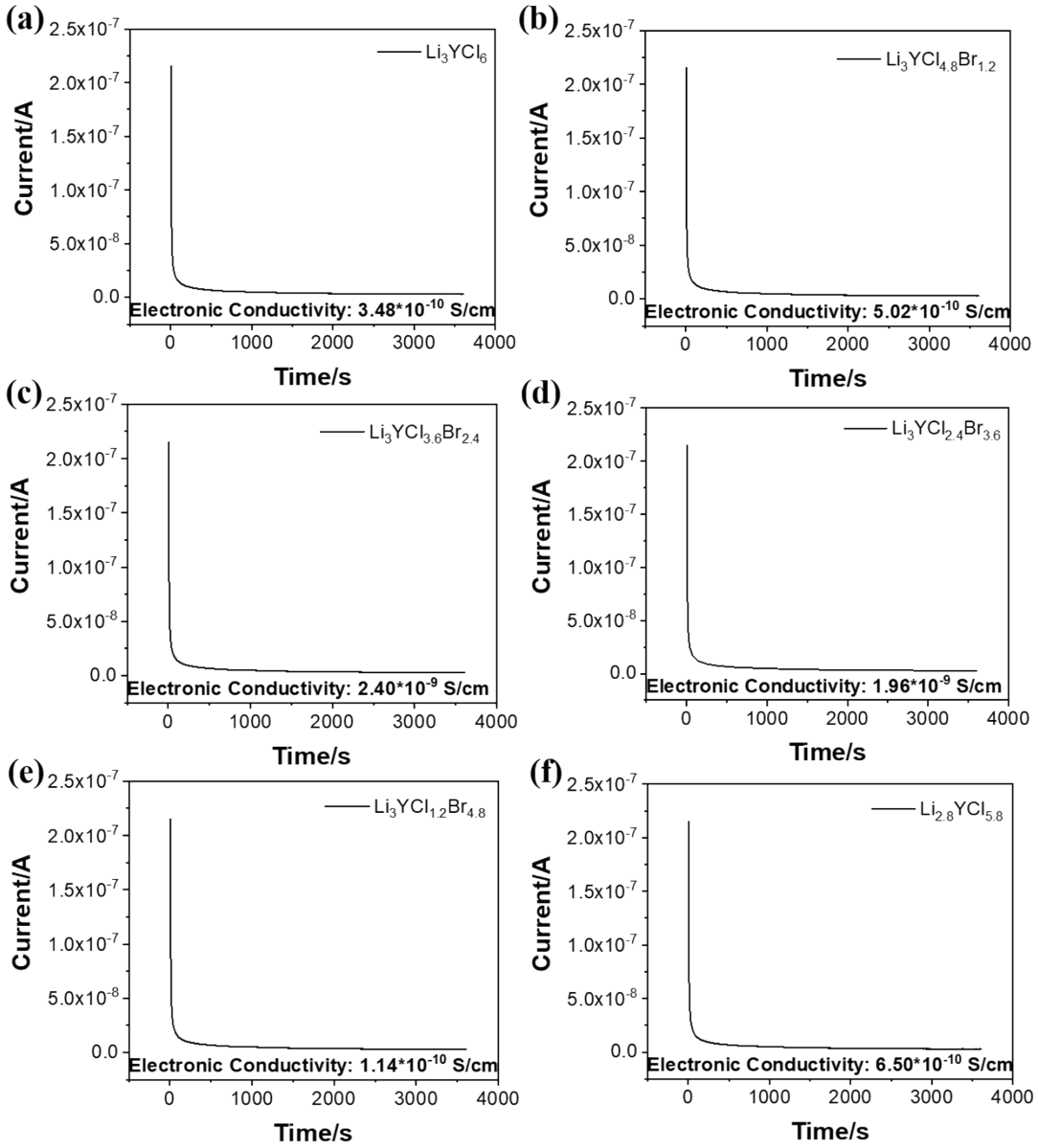

Figure S6. Chrono amperometry curves of (a) Li_3YCl_6, (b) $Li_3YCl_{4.8}Br_{1.2}$, (c) $Li_3YCl_{3.6}Br_{2.4}$, (d) $Li_3YCl_{2.4}Br_{3.6}$, (e) $Li_3YCl_{1.2}Br_{4.8}$, (f) $Li_{2.8}YCl_{5.8}$ at 1V voltage and 25℃.

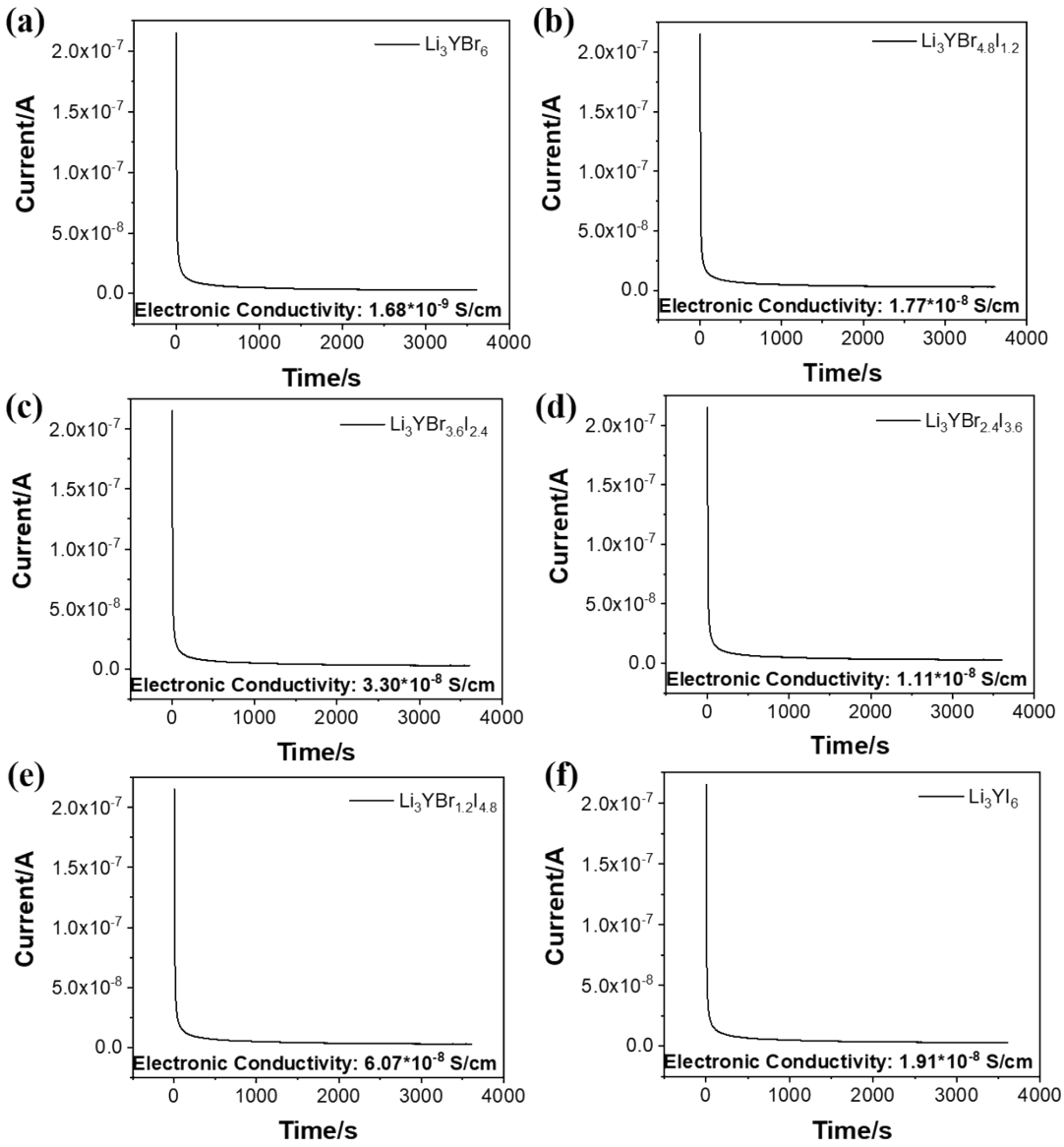

Figure S7. Chrono amperometry curves of (a) Li_3YBr_6, (b) $Li_3YBr_{4.8}I_{1.2}$, (c) $Li_3YBr_{3.6}I_{2.4}$, (d) $Li_3YBr_{2.4}I_{3.6}$, (e) $Li_3YBr_{1.2}I_{4.8}$, (f) Li_3YI_6 at 1V voltage and 25°C.

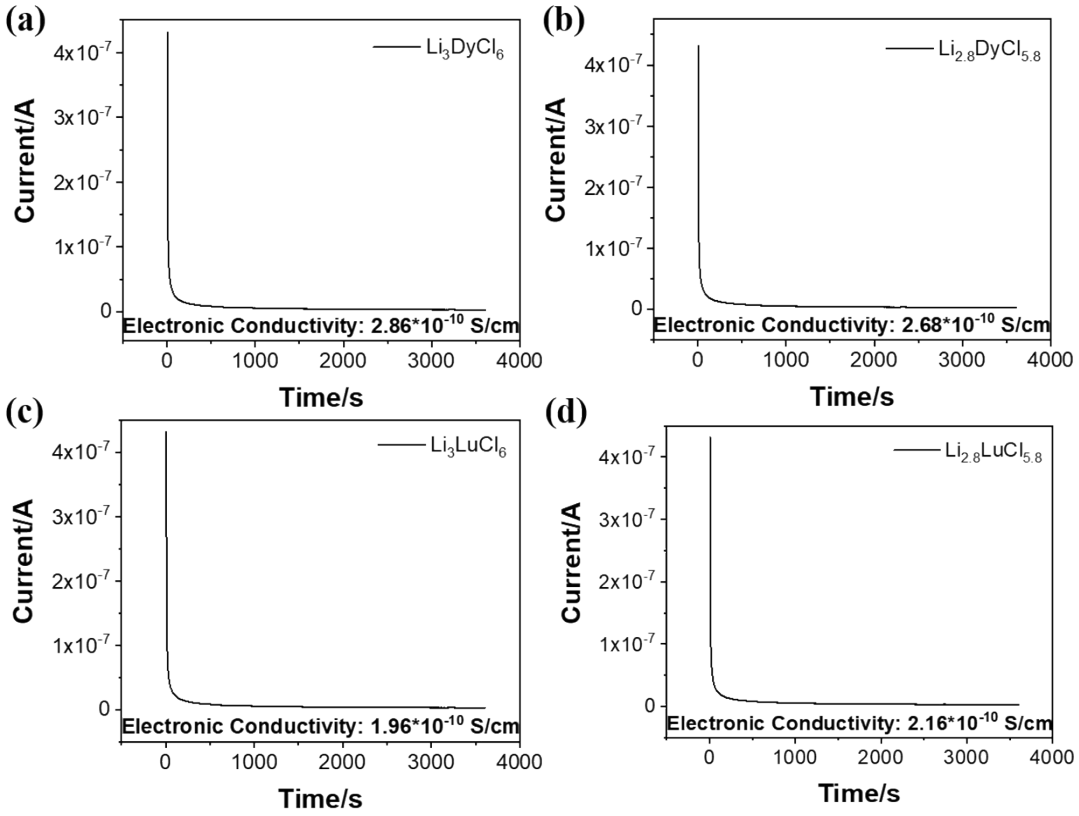

Figure S8. Chrono amperometry curves of (a) Li_3DyCl_6, (b) $Li_{2.8}DyCl_{5.8}$, (c) Li_3LuCl_6, (d) $Li_{2.8}LuCl_{5.8}$ at 1V voltage and 25℃.

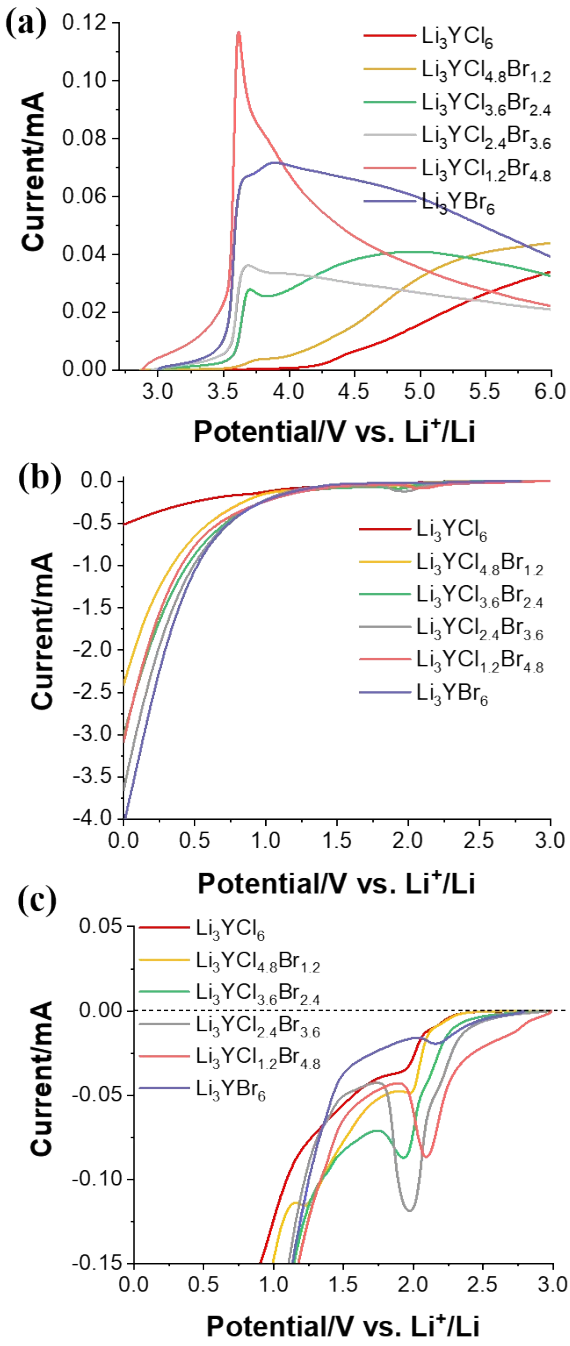

Figure S9. Linear sweep voltammetry (LSV) curves of $Li_3YCl_{6-x}Br_x$ (x=0, 1.2, 2.4, 3.6, 4.8, 6) with a scan range from the (a) open-circuit voltage (OCV) to 6V (vs Li/Li^+, position scan), (b) OCV to 0 V (vs Li/Li^+, negative scan), respectively. (c) Enlarged view of LSV curves with a scan range from OCV to 0 V.

Table S4. Electrochemical stability window of $Li_3YCl_{6-x}Br_x$ (x=0, 1.2, 2.4, 3.6, 4.8, 6)

Sample	Oxidation Potential	Reduction Potential
Li_3YCl_6	4.18	2.13
$Li_3YCl_{4.8}Br_{1.2}$	3.59	2.15
$Li_3YCl_{3.6}Br_{2.4}$	3.57	2.30
$Li_3YCl_{2.4}Br_{3.6}$	3.55	2.37
$Li_3YCl_{1.2}Br_{4.8}$	3.52	2.39
Li_3YBr_6	3.50	2.60

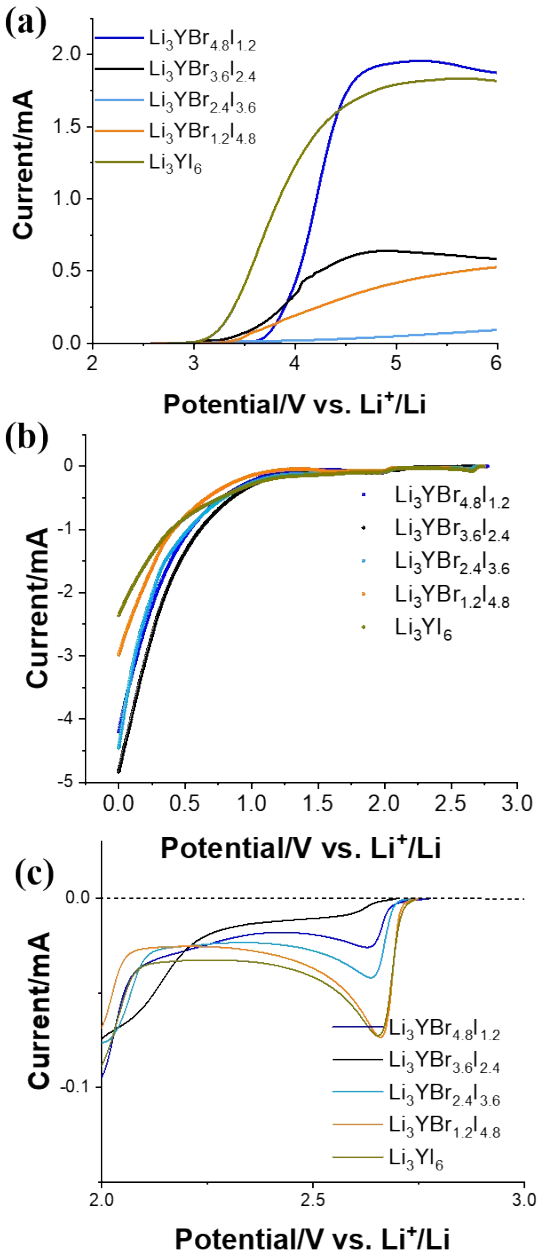

Figure S10. Linear sweep voltammetry (LSV) curves of $Li_3YBr_{6-x}I_x$ (x=1.2, 2.4, 3.6, 4.8, 6) with a scan range from the (a) open-circuit voltage (OCV) to 6V (vs Li/Li^+, position scan), (b) OCV to 0 V (vs Li/Li^+, negative scan), respectively. (c) Enlarged view of LSV curves with a scan range from OCV to 0 V.

Table S5. Electrochemical stability window of $Li_3YBr_{6-x}I_x$ (x=1.2, 2.4, 3.6, 4.8, 6).

Sample	Oxidation Potential	Reduction Potential
$Li_3YBr_{4.8}I_{1.2}$	3.78	2.68
$Li_3YBr_{3.6}I_{2.4}$	3.41	2.68
$Li_3YBr_{2.4}I_{3.6}$	3.40	2.69
$Li_3YBr_{1.2}I_{4.8}$	3.34	2.71
Li_3YI_6	3.28	2.72

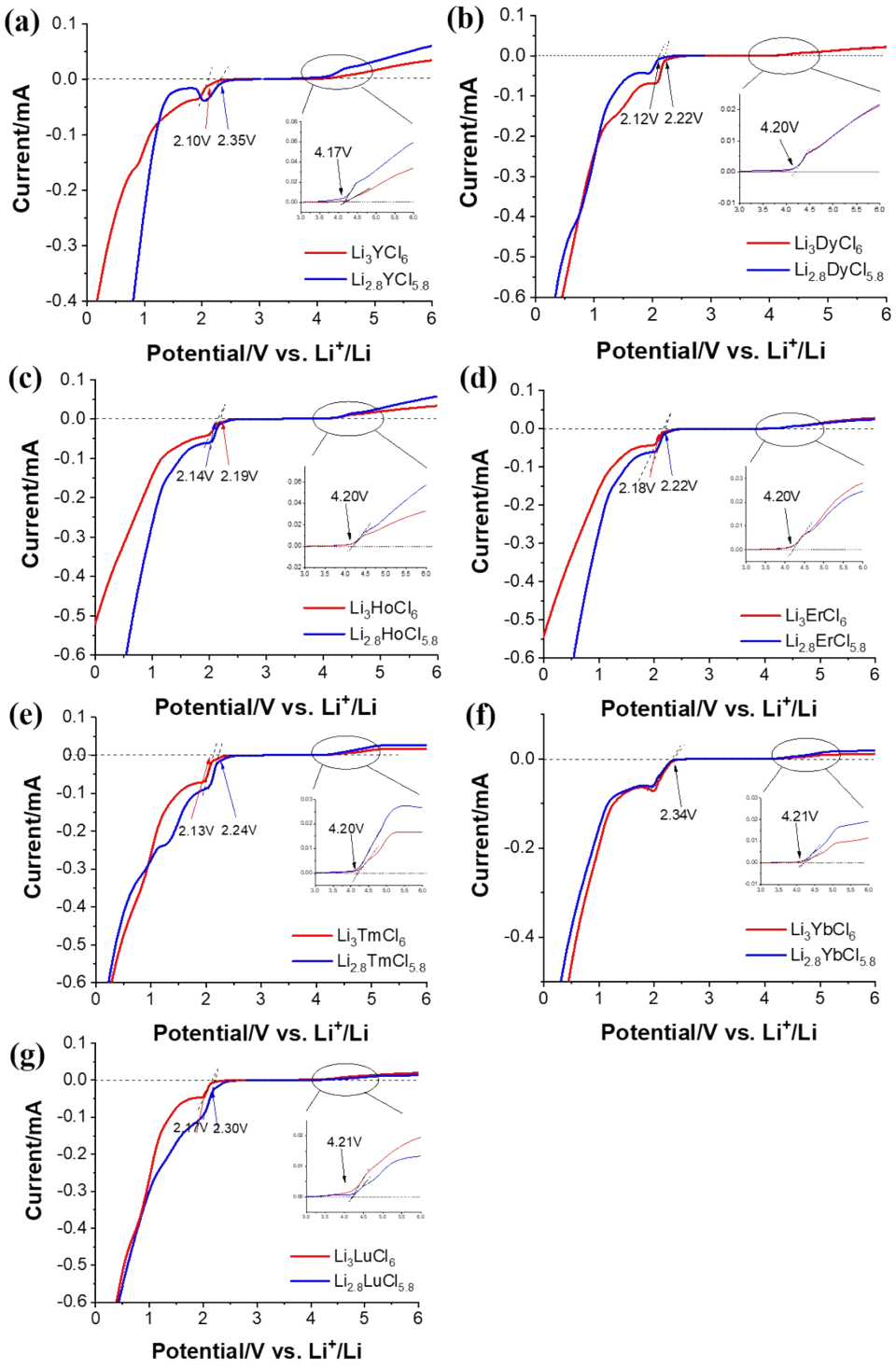

Figure S11. Linear sweep voltammetry (LSV) curves of Li_3MCl_{3+x} (x=3, 2.8) with a scan range from 0~6 V. (a) M=Y, (b) M=Dy, (c) M=Ho (d) M=Er, (e) M=Tm, (f) M=Yb, (g) M=Lu.

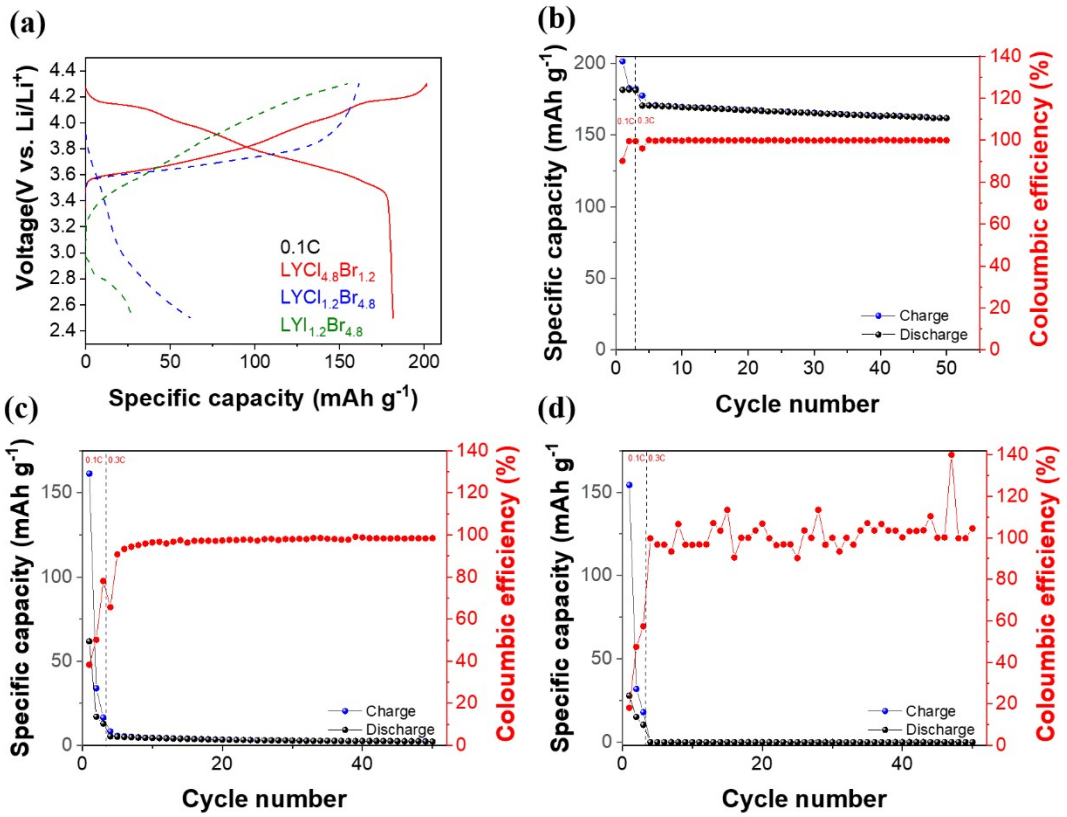

Figure S12. (a) First cycle data and (b-d) long term cycling performance of full cells using In-Li/$Li_{5.5}PS_{4.5}Cl_{1.5}$/halide SSE/SSE-NCM88: (b) $Li_3YCl_{4.8}Br_{1.2}$, (c) $Li_3YCl_{1.2}Br_{4.8}$, (d) $Li_3YI_{1.2}Br_{4.8}$. The batteries were cycled at 0.1C at the first three cycles, and cycled at 0.3C after the third cycle.

Reference

1 X. Li, J. T. Kim, J. Luo, C. Zhao, Y. Xu, T. Mei, R. Li, J. Liang and X. Sun, *Nat. Commun.*, 2024, **15**, 53-60.